

# Impact of multiple delays on the governance of risky commons

Ana M. Nunes<sup>1</sup>, Francisco C. Santos<sup>2,3</sup>, and Jorge M. Pacheco<sup>3</sup>

<sup>1</sup>*BioSystems and Integrative Sciences Institute, and Departamento de Física,*

*Faculdade de Ciências da Universidade de Lisboa Campo Grande, 1749-016 Lisboa, Portugal*

<sup>2</sup>*INESC-ID and Instituto Superior Técnico, Universidade de Lisboa, 2744-016 Porto Salvo, Portugal*

<sup>3</sup>*ATP-Group, P-2744-016 Porto Salvo, Portugal*



(Received 17 February 2025; accepted 5 June 2025; published 7 July 2025)

Long-time global cooperation is required to reduce CO<sub>2</sub> emissions towards controlling climate change, one of the most paradigmatic examples of a risky common. The problem has been often modeled, theoretically, employing the so-called Collective Risk Dilemma (CRD), a threshold public goods game in the presence of risk, which has been shown to play a crucial role. Up to now, however, the long delays that mediate (i) political decisions and their implementation, (ii) implementations and their effective emissions reduction, and (iii) emissions reduction and risk assessment, have been largely ignored. Here we investigate how these multiple delays affect overall cooperation, by analyzing the evolutionary game dynamics of a recently developed variant of the CRD model where the dynamical feedback between risk and cooperation is incorporated. We show how the consideration of multiple, incremental delays may lead to scenarios that range from the conventional wisdom of straight delay-intrinsic destabilization of otherwise stable fixed points, to scenarios in which additional delays may limit the impact of delay-intrinsic destabilization. We trace these different outcomes back to the scaling relation between risk feedback and cooperation and discuss under which conditions multiple delay effects may actually foster global cooperation.

DOI: [10.1103/782p-l2bq](https://doi.org/10.1103/782p-l2bq)

## I. INTRODUCTION

The Kyoto protocol (1997) and the Paris Agreement (2015) have earned so much popularity that nowadays they have been incorporated into the folklore of global warming. Yet, 8 years after Paris, the Copernicus observatory announced that “We’ve ‘lost’ 19 years in the battle against global warming since the Paris Agreement” [1] based on linear extrapolation of longitudinal data on Earth’s average temperature. This is but one example of a large corpus of information stating that the effects of political decisions take too long to implement, leading to sizable deviations from targets initially determined. Indeed, it is now clear that when dealing with climate change, time intervals between cause and effect are best measured in decades rather than years, with implications that are yet to be understood. The Copernicus news relates what we may designate by original cause—political decision—and (ultimate) effect—Earth average temperature. However, there is a long ongoing process mediating the original cause and the ultimate effect. First, as stated, political decisions take time to be implemented. Second, implementation takes (a long) time to produce measurable effects, in particular, those derived from reduced CO<sub>2</sub> emissions [2]. Third, the level of widespread adherence to political decisions, together with the impact of their effects on global emissions, also influences the assessment of the risk of failing to meet the targets originally agreed upon. Risk assessment, in turn, should not be overlooked, as it feeds back into countries’ willingness to cooperate to reduce global warming, thereby influencing future decisions. Here we investigate the impact of these time intervals between causes, effects, and feedbacks making use of a recently developed variant of the original Collective Risk Dilemma (CRD) [3]

that we designate by Risk-Feedback CRD [4] (RFCRD) where risk, shown to play a crucial role as a fixed, external parameter in the CRD, now becomes a dynamical feedback variable of the model. This approach provides perhaps the simplest workable framework in which to investigate the multiple delay problem discussed above (compare with a related framework developed in Ref. [5]). As a threshold public goods game [3,6], an evolutionary game theoretical investigation of the RFCRD leads to a nonlinear dynamical system problem. The effects of delay in this type of system have been investigated to some extent [7–11], but results obtained so far cannot account for the multiple types of delays we address here. The general message is that delays imposed on dynamical systems do not change the location of the fixed points of the dynamics, but typically act to reduce the stability of otherwise stable fixed points of the system. In general, there is a limit above which these equilibria lose stability due to the appearance of a Hopf bifurcation [7]. We will show, in the following, how the consideration of incremental delays acts to change the stability patterns of the system in fundamental ways, and we shall characterize the limits within which the stability of the system survives. As a result, the present model will allow us to understand in detail the role of multiple delays in the dynamics, in particular, how they may reduce or enlarge both the regions of stability and the basins of attraction of the cooperative regimes which, as we also show, depend on how risk feedback scales with cooperation.

## II. MODEL

Let us consider, for simplicity, an infinite, well mixed population of individuals who engage in a threshold Public

Goods game characterized by a limited set of behaviors: to Cooperate ( $C$ ) or to defect ( $D$ ). Players each have an initial endowment  $b$ . Cooperators ( $C$ s) contribute a fraction  $c b$  of their endowment (where  $c$  stands for the cost-to-benefit ratio) while defectors ( $D$ s) do not contribute. Furthermore, we require a minimum collective investment (threshold) to ensure any benefit: If a group of size  $N$  does not contain at least  $M$   $C$ s, all members will lose their remaining endowments with a probability  $r$  (the global risk perception) [3]; otherwise everyone will keep whatever they have. Rational players facing this one-shot dilemma will opt for defection, as  $D$ s never get a lower payoff in mixed groups. However, this reasoning ignores the collective (populationwide) dynamics, where a continuous (and eventually long-term) process of behavioral revision takes place [3,12–14]. In an evolutionary game theory (EGT) formulation [15,16], individuals tend to copy others whenever these appear to be more successful, allowing policies to change as time goes by, likely influenced by the behavior (and achievements) of others. In this framework, the evolution of the fraction  $x$  of  $C$ s (and  $1 - x$  of  $D$ s) in a large population is governed by the gradient of selection associated with the replicator dynamics equation [15,16]  $\dot{x} = x(1 - x)(f_C - f_D)$  characterizing the behavioral dynamics of the population, where  $f_C$  ( $f_D$ ) is the fitness of  $C$ s ( $D$ s), here associated with the average game payoffs of each player type in the population. According to the replicator equation,  $C$ s ( $D$ s) will increase (decrease) in the population whenever  $\dot{x} > 0$  ( $\dot{x} < 0$ ). Random sampling leads to groups whose composition follows a binomial distribution. Hence we may write for the fitness of  $C$ s and  $D$ s

$$f_C(x) = \sum_{k=0}^{N-1} \binom{N-1}{k} x^k (1-x)^{N-1-k} \Pi_C(k+1)$$

and

$$f_D(x) = \sum_{k=0}^{N-1} \binom{N-1}{k} x^k (1-x)^{N-1-k} \Pi_D(k),$$

where  $\Pi_C(k)$  [ $\Pi_D(k)$ ] stands for the payoff of a  $C$  ( $D$ ) in a group of size  $N$  with  $k$   $C$ s. The payoff of a  $D$  can be written as

$$\Pi_D(k) = b\{\theta(k - M) + [1 - r(\eta)][1 - \theta(k - M)]\},$$

where  $\theta(x) = 0$  if  $x < 0$ , and 1 otherwise, whereas the payoff of a  $C$  is given by

$$\Pi_C(k) = \Pi_D(k) - c b \quad (0 < c \leq 1),$$

and where  $0 \leq M \leq N$  stands for the coordination threshold [3,6] necessary to produce a collective benefit. In the RFCRD [4], risk becomes a function of  $x$  via the fraction of groups that have  $k \geq M$   $C$ s, which we denote by  $\eta(x)$ ,

$$\eta(x) = \sum_{k=M}^N \binom{N}{k} x^k (1-x)^{N-k}.$$

For  $r(\eta)$  we retain the essential parametric dependence introduced in [4] and write  $r[\eta(x); \sigma] = [1 - \eta(x)]^\sigma$ . This scaling leads to a single nonlinear differential equation (see below) describing the risk-feedback dynamics, as opposed to the related framework of Ref. [5] where a system of two coupled

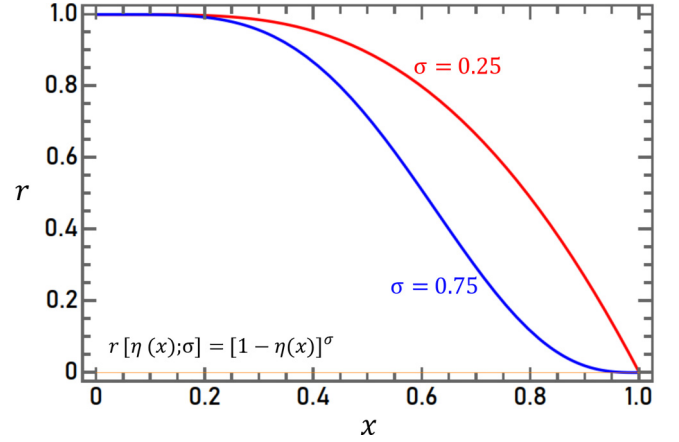


FIG. 1. Risk dependence on cooperation. Risk ( $r$ ) is plotted as a function of the fraction ( $x$ ) of cooperators in the population for two values of the parameter  $\sigma$  that controls how  $r$  scales with  $x$  (see equation shown in the figure):  $\sigma = 0.25$  (red curve) and  $\sigma = 0.75$  (blue curve). These two curves portray two different scenarios describing how risk changes with cooperation: For  $\sigma = 0.25$  risk declines slowly with increasing cooperation (and increases rapidly as cooperation decreases). For  $\sigma = 0.75$  risk declines faster with increasing cooperation compared to  $\sigma = 0.25$ .

nonlinear differential equations was set up to describe a similar dynamical risk-feedback process in the absence of delay.

Figure 1 illustrates the role of the parameter  $\sigma$  in characterizing the scaling feedback between risk and cooperation. As shown in Fig. 1, risk ( $r$ ) declines with increasing cooperation ( $x$ ). However, when  $\sigma = 0.25$  risk decreases slower with increasing cooperation compared to the scaling  $\sigma = 0.75$ , which provides a more optimistic scenario. Indeed, high risk is known to foster cooperation in the CRD [3]. In the following we shall investigate the effects of imposing different delays using the two  $\sigma$  values depicted in Fig. 1. In Fig. 2 we set the stage by examining the evolutionary dynamics of the RFCRD in the absence of delay. Inclusion of delay(s) will change the scenario portrayed in panels (b)–(d) of Fig. 2, though not the structure of four fixed points depicted in panel (a), which characterize the evolutionary dynamics: (a) (defective) stable fixed point (DS) at full defection ( $x = 0$ ), an internal unstable fixed point (IU) at  $x = 0.305$ , an internal stable fixed point (IS) at  $x = 0.751$ , and, finally, a (cooperative) unstable fixed point (CU) at full cooperation ( $x = 1$ ).

In line with the discussion above, the rate of change of behavior at time  $t_0$ ,  $\dot{x}(t_0)$  will result from a population behavior (dictated by fitness in the RFCRD) at a previous time  $t_1 = t_0 - \tau$  ( $\tau \geq 0$ ), when decisions were taken. Moreover, these decisions, in turn, were based on a risk assessment which was made eventually before, at some relative time  $t_2 = t_1 - \delta$  ( $\delta \geq 0$ ). This means that the replicator equation, with these incremental delays included, formally reads

$$\begin{aligned} \dot{x}(t) = & x(t)(1 - x(t))[f_C\{x(t - \tau), r[x(t - \tau - \delta)]\} \\ & - f_D\{x(t - \tau), r[x(t - \tau - \delta)]\}]. \end{aligned} \quad (1)$$

It is worth noting that, similar to Ref. [7], Eq. (1) leaves invariant the number and location of interior fixed points of the evolutionary dynamics. As discussed in Ref. [17], this

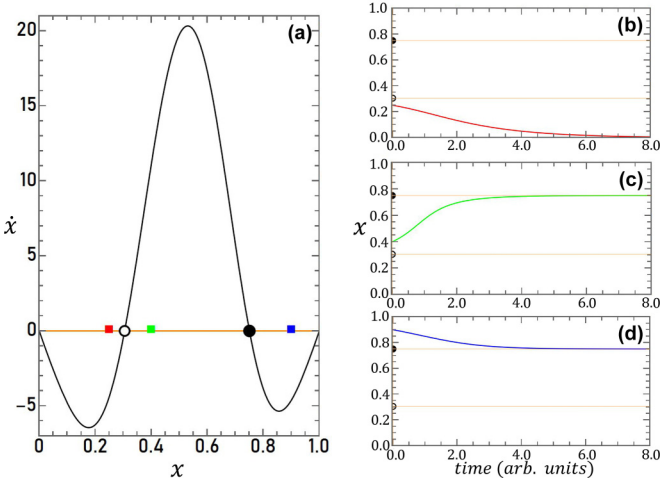


FIG. 2. Evolutionary dynamics without delay. (a) Gradient of selection ( $\dot{x}$ ) as a function of the fraction of Cs ( $x$ ) in the population making use of the RFCRD model (which includes risk feedback in the form  $r[\eta(x)]$ ; cf. Fig. 1). The solid black circle indicates the location of the IS ( $x = 0.751$ ) of the dynamics, leading to a coexistence of  $\approx 75\%$  Cs with  $\approx 25\%$  Ds; the open black circle indicates the location of the IU ( $x = 0.305$ ) of the dynamics. Two additional fixed points characterize the evolutionary dynamics: the CU ( $x = 1$ ) and the DS ( $x = 0$ ). This structure of dynamic equilibria is a characteristic feature of threshold public goods games and the RFCRD is no exception. The right panels show how the evolution of the fraction of Cs in time depends on the initial fraction of Cs one starts with [indicated with colored squares in (a)]: (b) below the IU (red); (c) between the IU and the IS (blue); (d) above the IS (green). As expected, only starting below the IU will lead to a collapse of cooperation, all other scenarios leading to a relaxation to the IS. Model parameters used:  $b = 5.475$ ,  $c = 0.1$ ,  $N = 8$ ,  $M = 5$ ,  $\sigma = 0.25$ , leading to a characteristic relaxation time  $\tau_\omega \simeq 1$  time unit (see Sec. 2 of the Supplemental Material (SM) [18]).

so-called social-type model is not the only way one may include delay effects in evolutionary models, in which case such invariance no longer necessarily holds [11,19].

### III. RESULTS

Let us start by investigating the effect of a single, common delay in the replicator equation. The standard form [7] assumes that present behavior derives from a fitness computed before, with a single delay  $\tau$  [ $\delta = 0$  in Eq. (1)]. Applying Linear Response Theory [7] to the delay terms in Eq. (1) assumes that deviations  $y$  from the IS—see black solid circle in Fig. 2—have the form  $y = e^{\omega t}$ , leading to a behavior of the (complex)  $\omega$  as a function of the delay  $\tau$  illustrated in Fig. 3(a) (we made  $\delta = 0$  and used the model parameters of Fig. 2), predicting that for  $0 \leq \tau < \tau_H \equiv 1.57$  the IS (at  $x = 0.751$ ) is asymptotically stable, whereas at  $\tau_H$  a Hopf bifurcation occurs, at which point undamped oscillations around the IS emerge [Fig. 3(b)], whose amplitude increases as  $\tau$  increases until ultimately all trajectories end in the DS [Fig. 3(d)]. Furthermore, with increasing  $\tau$ , the frequency of the oscillations is expected to decrease, associated with the decline of the imaginary part of  $\omega(\tau)$  shown in Fig. 3(a) (for additional

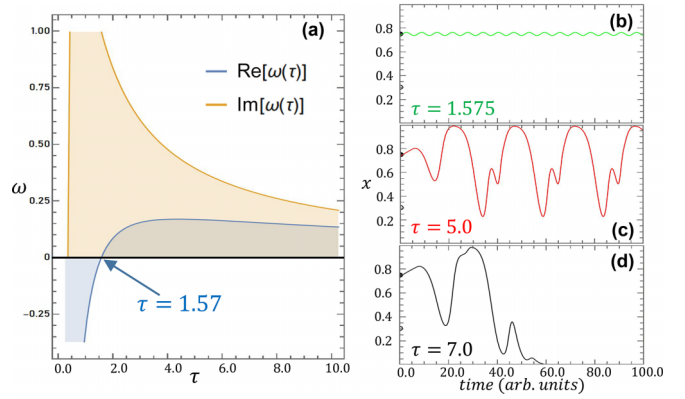


FIG. 3. Linear Response predictions and numerical simulations. Linear Response Theory assumes that deviations from the IS behave as  $y = e^{\omega t}$  where  $\omega$  becomes a (complex) function of the delay  $\tau$  (see SM Sec. 2 [18]). Here we made  $\delta = 0$  in Eq. (1). Panel (a) illustrates the behavior of the real and imaginary parts of  $\omega(\tau)$ . When  $\tau = \tau_c = 1.57$  a Hopf bifurcation occurs, as the real part of  $\omega$  crosses zero, leading to stable oscillations around the IS whose frequency is expected to decrease with increasing  $\tau$ . (b) Numerical integration of Eq. (1) for  $\tau = 1.575$ ,  $\delta = 0$ , right above the Hopf bifurcation, exhibiting undamped oscillations in the vicinity of the IS (indicated with a black solid semicircle, with the IU indicated with a black open semicircle). (c), (d) Same as (b) computed for higher values of  $\tau$  showing that for  $\tau \geq 7$  the system converges to the DS. In all panels we used the same parameters as in Fig. 2 and  $x(\tau \leq 0) = 0.74$ .

details see Sec. 2 of the Supplemental Material (SM) [18], where we also show, in Fig. S1, the behavior of  $\omega(\tau)$  for  $\sigma = 0.75$ ).

As shown in Fig. 3(b), the predictions of the linear approximation (cf. Sec. 2 of the SM [18] for details) hold compared to the numerical integration of Eq. (1). Moreover, for  $\tau > 4$  increasingly complex oscillation patterns are observed [Fig. 3(c)], ultimately leading to the demise of cooperation [Fig. 3(d)]. It is noteworthy that the DS at  $x = 0$  is always a stable fixed point of the overall dynamics, and for  $\tau > 4$  it becomes the only attractor. The same qualitative scenario is obtained for  $\sigma = 0.75$ , except in what concerns the locations of the interior fixed points and critical delay values, as shown in the SM in a corresponding figure (Fig. S1 [18]). It is important to note (cf. caption to Fig. 2) that the value of the RFCRD game parameter  $b$  was chosen, in all cases, so that deviations from the IS in the absence of delay will relax to the IS with a characteristic timescale of 1, which may be conveniently used as a reference timescale with which to compare the critical values  $\tau_H$  discussed here.

Equation (1) with  $\delta = 0$  portrays a scenario in which risk assessment is made instantaneously. This simpler, yet unrealistic, scenario leads to results that are qualitatively independent of how risk feedback scales with cooperation (as determined by the parameter  $\sigma$ ). This becomes apparent when comparing Fig. 3 and Fig. S1 of the SM [18], and provides a *conventional wisdom* scenario of delay-intrinsic destabilization of otherwise stable fixed points of the evolutionary dynamics, in line with previous studies of delay effects in evolutionary games [7–11].

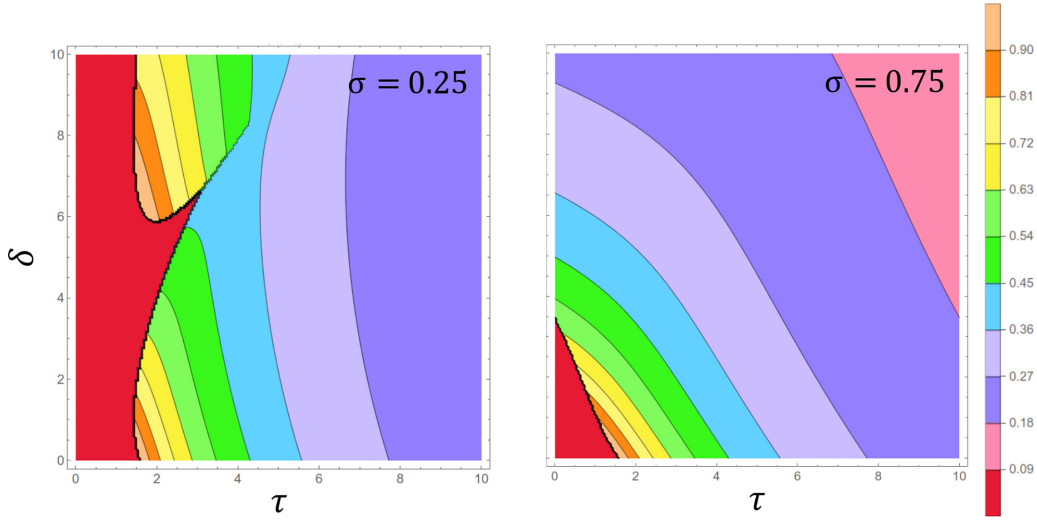


FIG. 4. Linear Response predictions for different delays. Left: Contour plot of  $\text{Im}[\omega(\tau, \delta)]$  computed for the model parameters of Fig. 1 where  $\sigma = 0.25$ . The red colored regions are associated with a stable regime in the vicinity of the cooperative IS (in which case we have  $\text{Re}[\omega(\tau, \delta)] < 0$ ). One observes that for small  $\delta > 0$  the interval in  $\tau$  for which the system is stable decreases, increasing when  $1 \leq \delta \leq 5.5$ , at which point a new bifurcation occurs, further destabilizing the system (see main text for details). Right: Same as in the Left panel but with  $\sigma = 0.75$ . In this case, one observes that increasing  $\delta$  acts to destabilize the IS. The results shown here, however, cannot provide a general picture of the evolutionary dynamics, as they typically portray the behavior associated with small deviations from the cooperative IS, whereas in general we are not close to the IS.

Let us now consider the more general case of Eq. (1) in which we have now two nonzero, incremental delays,  $\tau$  and  $\delta$ . Linear Response Theory applied to this case is considerably more complex and requires the numerical solution of complex transcendental equations (see SM Sec. 2 [18] for details).

In Fig. 4 we show the results for  $\text{Im}[\omega(\tau, \delta)]$  obtained when  $\sigma = 0.25$  (left panel) and  $\sigma = 0.75$  (right panel), evidencing a very different behavior for these two risk-feedback scaling regimes, in sharp contrast with what was obtained for a single nonzero delay  $\tau$ .

The red regions in both panels are associated with the values  $\text{Re}[\omega(\tau, \delta)] < 0$ ; that is, they represent regions where the delays do not affect the original dynamics of the system—at most, damped oscillations to the IS take place. Clearly, along the axis  $\delta = 0$  one observes the behavior already discussed before. The right panel of Fig. 4 (associated with  $\sigma = 0.75$ ) shows that, with increasing  $\delta$ , the stability of the IS due to two incremental delays is always worse compared to the case  $\delta = 0$ . The left panel of Fig. 4 (associated with  $\sigma = 0.25$ ), on the contrary, portrays a more stable scenario as, overall, one expects that in the region  $\delta > 0$ , the IS may exhibit a higher stability compared to the  $\delta = 0$  regime.

Only in the interval  $0 \leq \delta \leq 1$  is the window of stability of  $\tau$  (for fixed  $\delta$ ) (marginally) smaller than for  $\delta = 0$ . For  $1 \leq \delta \leq 5.5$  the window of stability of  $\tau$  increases with  $\delta$  until for  $\delta \sim 6$  it becomes disconnected (moving horizontally) and subsequently recovers the range of stability in  $\tau$  already observed for low  $\delta$ .

However, to provide a more complete description of the global dynamics, we must explore how the system behaves not only away from the Hopf bifurcation boundary, but also in scenarios where we start far from the IS (abandoning the assumption of small deviations implicit in Linear Response Theory—yet, hopefully already in the basin of attraction of

the IS) which mimic more realistically the present World situation, where we are far from (and below) the IS.

The results are shown in Fig. 5, where we integrated numerically Eq. (1) spanning a discrete grid in the  $(\tau, \delta)$  parameter space while starting from different initial conditions (cf. top panels in Fig. 5 and Sec. 1 of the SM [18]), computing also, at each grid point, the associated Fourier spectrum of the time series. We discarded an initial transient in the computation of the Fourier Transform in order to identify numerically the long-term attractors of the system, be they single points, periodic orbits, or chaotic attractors, whose signature is, asymptotically, associated with aperiodic behavior.

Comparing the three panels in Fig. 5, we see that in order not to miss small amplitude damped or undamped oscillations around the IS we must choose initial conditions corresponding to small deviations from the IS. The results show that one recovers the red region in Fig. 4 associated with the IS as the final attractor, even in regimes where it can compete with the DS at  $x = 0$ . According to Linear Response Theory, and similar to the case  $\delta = 0$ , whenever one crosses the black boundary depicted in Fig. 4, the system undergoes undamped oscillations around the IS, whose frequency is predicted to decrease with increasing  $\tau$ .

Upon numerical integration of Eq. (1), however, we observe a somewhat different scenario. Indeed, at the boundary of the red zone and the blue zone in Fig. 5, the cooperative attractor becomes a stable periodic orbit, whose frequency is approximately given by the imaginary part of the solution of the corresponding transcendental equation (SM, Eq. (S3) [18]). This approximation of course deteriorates as one moves away from the boundary of the red region and the amplitude of the stable oscillations increases. As shown in Fig. 5, undamped oscillations associated with the blue dots evolve towards a new boundary with a back region where cooperation



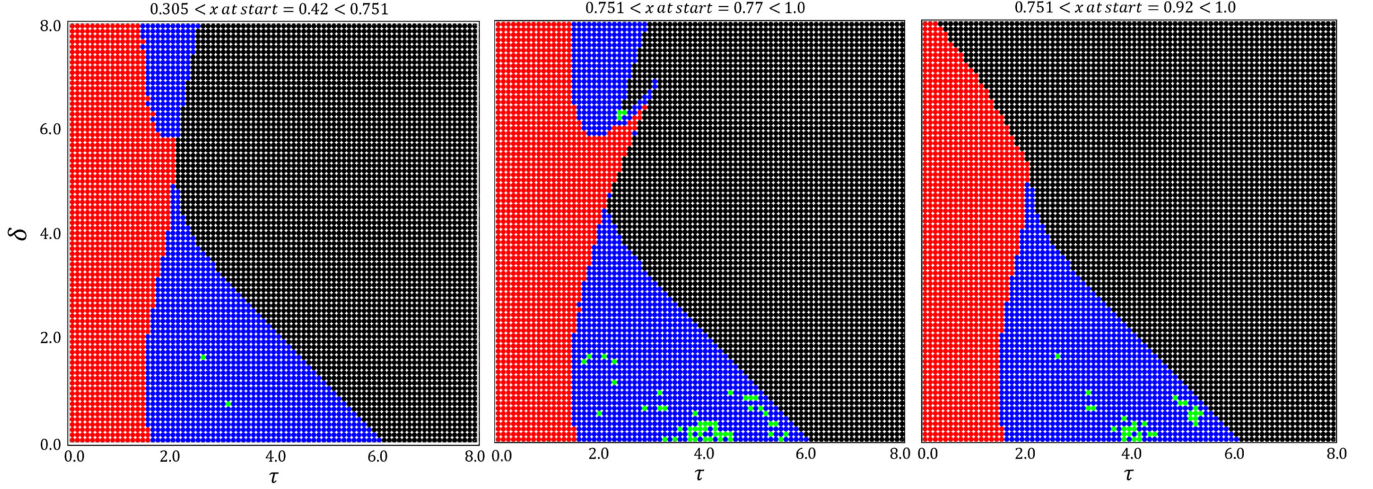


FIG. 5. Time integration of Eq. (1). Time integration of Eq. (1) was carried out for a long time period ( $t = 10\,000$ ). We used the parameters of Fig. 2 and selected a discrete grid of delay values, where  $0 \leq \tau, \delta \leq 8$  using  $\Delta\tau = \Delta\delta = 0.1$ . Besides the time integration we also performed a Fast Fourier Transform of the time series after discarding a first transient up to  $t = 1000$ . This way, we can easily identify the long-term attractors of the system, be they single points (such as IS or DS), periodic orbits, or chaotic attractors, whose signature is, asymptotically, associated with aperiodic behavior. Relaxation (with or without damped oscillations) to the IS is represented by red solid circles. Undamped oscillations around the IS are represented with solid blue circles. Relaxation (with or without damped oscillations) to the DS are shown with black solid circles. Finally, green solid circles indicate instability of the numerical integration algorithm. Left: Results obtained for time integration starting at  $x = 0.42$ , close to the location of the IU at  $x = 0.305$  but already in the basin of attraction of the IS located at  $x = 0.751$  (cf. top of panel). Middle: Same as the Left panel but starting from  $x = 0.77$  (cf. top of panel), close but already above the IS. Right: Same as the Left and Middle panels but starting from  $x = 0.92$  (cf. top of panel), already well above the IS. Starting in the vicinity of the IS (Middle) leads to the pattern that most resembles that obtained from Linear Response Theory shown in Fig. 4(a) in what concerns the red-blue border. However, the blue-black border indicates (all panels) the occurrence of another bifurcation by which the periodic orbit disappears, leading to the demise of cooperation.

disappears. Inspection of the behavior of the solutions on the blue region close to this blue-black boundary (exemplified in Fig. 6) shows that the transition takes place through a ho-

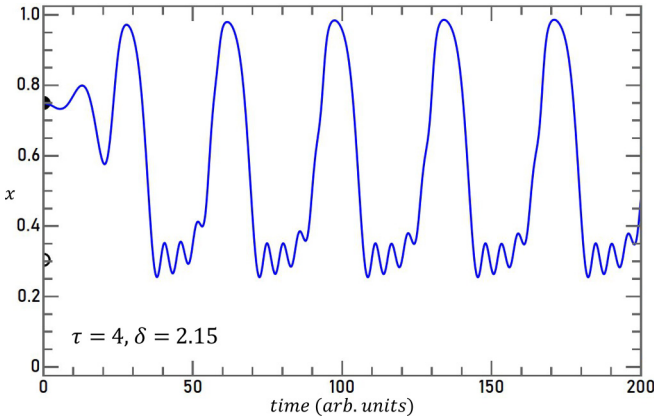


FIG. 6. Time series for  $x(t)$ . We show the time evolution of  $x(t)$  using the model parameters of Fig. 2 where  $\sigma = 0.25$ . Starting close to the IS (black solid semicircle), for the values of delays  $\tau$  and  $\delta$  indicated, we observe that the amplitude of the periodic orbit is large enough to reach the IU (black open semicircle). The resulting interaction leads to a perturbation of the original oscillatory behavior which, for these values of  $\tau$  and  $\delta$ , is not yet strong enough to destroy the periodic behavior. As we further increase  $\delta$  or, alternatively, as we start further away from the IS, the population will converge to the DS.

moclinic bifurcation—the periodic orbit ceases to exist after colliding with the IU at  $x = 0.305$ . Overall, the large-scale numerical integration of Eq. (1) shows that, in what concerns the long-term behavior of the dynamics, three main regimes emerge, common to both risk-feedback scalings considered here, whenever one starts within the basin of attraction of the IS (in the absence of delay): stability, periodic behavior, and collapse of cooperation. These behaviors are not affected qualitatively by changing the structure of the initial conditions implemented in solving Eq. (1) (the results shown correspond to assuming constant behavior for  $t \leq 0$ ).

#### IV. DISCUSSION

As stated in the Introduction, there is a large corpus of information, both research data and media coverage of the detrimental effects of climate change, which have raised an acute awareness of the associated risks. Moreover, the limited success of Global Climate Summits, as widely perceived, has brought in some skepticism regarding any announcement of success in fighting Global Warming. Both factors contribute, in our opinion, to favor a scenario for risk-feedback scaling more akin to  $\sigma = 0.25$ , where risk decline rate with increasing cooperation is lower than that associated with  $\sigma = 0.75$ . This is good news since, as shown in Figs. 4 and 5, the stability regime is much more insensitive to the (inevitable) delays in risk assessment. On the other hand, the present urgency in fighting Global Warming prompts for an analysis

of short-term behavior, as opposed to long-term behavior. In this respect, it is important to note that we “calibrated” our RFCRD model to relax to the internal stable fixed point with a characteristic timescale of 1 in the absence of delay (see caption of Fig. 2 and Sec. 2 of the Supplemental Material [18]). Clearly, nobody knows to which number this 1 should be compared with in the real world, more so if we take into consideration that any internal stable fixed point is undergoing permanent change as we speak. Nonetheless, our model indicates that for delays in  $\tau$  as small as roughly twice that of the calibrated timescale, we are already in an oscillatory regime. In other words, it is likely that, at present, we are undergoing an oscillating pattern of cooperation, whose frequency and amplitude will depend sensitively on the actual delay  $\tau$  between political decisions and their implementation, and not so much on the delay  $\delta$  between risk assessment and political decision, which is expected to decrease in time, as science progresses and more data become available. All together the present situation may support an oscillating pattern which allows for sustained oscillations of cooperation, whose amplitude, as shown in Fig. 3, may reach values of  $x$  arbitrarily close to the limit  $x = 1$ , that is, full cooperation. Needless to say, this feature of the dynamics is a consequence of the infinite population size implicit in Eq. (1). A more realistic scenario encompasses a stochastic dynamics involving finite populations (with sizes on the order of hundreds) [3,4,20,21], as opposed to the deterministic dynamics employed here. In other words, in realistic cases involving finite populations, large amplitude oscillations may eventually lead to the fixation into the extreme fixed points (CU at  $x = 1$  or DS at  $x = 0$ ). Given the fact that we are still far below the model IS, and given the past trajectory in addressing Global Warming, it is likely that we are in a first period of increasing cooperation, and in this sense, we may approach the CU before any possible collapse to the DS. Translating the behavior of our model into

a finite population paradigm [7], getting very close to the CU may actually mean reaching this configuration which, however, is dynamically unstable, and thus any perturbation will drive the population away from it. As shown in the right panel of Fig. 5, the ensuing dynamics may, in extreme cases, lead to the collapse of cooperation, although this less optimistic scenario will still take quite some time (many time units; cf. Fig. 3) to occur.

In summary, delay effects in the coevolutionary dynamics of risk and cooperation lead to a plethora of behaviors that may differ substantially not only for different delay values but also in what concerns short-term versus long-term behavior. The Hopf bifurcation that we observe in all cases, leading to the emergence of periodic orbits with amplitudes that tend to increase with increasing delays, can be superseded by a homoclinic bifurcation by which the periodic orbit ceases to exist and the collapse of cooperation ensues, a scenario that will be perturbed by stochastic effects in finite populations. At present, our model suggests that we may be undergoing an oscillatory regime along a trajectory of increasing cooperation, and it is up to us to decrease the effective delay between decision and implementation ( $\tau$ ) in order to avoid a full collapse of cooperation.

#### ACKNOWLEDGMENT

This research was supported by Fundação para a Ciência e a Tecnologia Portugal (PTDC/MATAPL/6804/2020, UIDB/50021/2020 and UIDB/04046/2020).




#### DATA AVAILABILITY

The data that support the findings of this article are openly available [22].

- 
- [1] Copernicus Climate Change Service, We’ve ‘lost’ 19 years in the battle against global warming since the paris agreement (2023), <https://tinyurl.com/yc42hvcn>.
  - [2] A. Buis, The atmosphere: Getting a handle on carbon dioxide, NASA Science Editorial Team (2019), <https://tinyurl.com/5fstdxra>.
  - [3] F. C. Santos and J. M. Pacheco, Risk of collective failure provides an escape from the tragedy of the commons, *Proc. Natl. Acad. Sci. USA* **108**, 10421 (2011).
  - [4] J. M. Pacheco and F. C. Santos, Co-evolution of risk and cooperation in climate policies under wealth inequality, *PNAS Nexus* **3**, pgae550 (2024).
  - [5] L. Liu, X. Chen, and A. Szolnoki, Coevolutionary dynamics via adaptive feedback in collective-risk social dilemma game, *Elife* **12**, e82954 (2023).
  - [6] J. M. Pacheco, F. C. Santos, M. O. Souza, and B. Skyrms, Evolutionary dynamics of collective action in  $n$ -person stag hunt dilemmas, *Proc. R. Soc. B* **276**, 315 (2009).
  - [7] J. A. Moreira, F. L. Pinheiro, A. Nunes, and J. M. Pacheco, Evolutionary dynamics of collective action when individual fitness derives from group decisions taken in the past, *J. Theor. Biol.* **298**, 8 (2012).
  - [8] S. Roy, S. Nag Chowdhury, S. Kundu, G. K. Sar, J. Banerjee, B. Rakshit, P. C. Mali, M. Perc, and D. Ghosh, Time delays shape the eco-evolutionary dynamics of cooperation, *Sci. Rep.* **13**, 14331 (2023).
  - [9] F. Yan, X. Chen, Z. Qiu, and A. Szolnoki, Cooperator driven oscillation in a time-delayed feedback-evolving game, *New J. Phys.* **23**, 053017 (2021).
  - [10] J. Miekisz, Evolutionary game theory and population dynamics, in *Multiscale Problems in the Life Sciences, From Microscopic to Macroscopic*, Lecture Notes in Mathematics Vol. 1940 (Springer, Berlin, 2008), pp. 269–316.
  - [11] M. Bodnar, J. Miekisz, and R. Vardanyan, Three-player games with strategy-dependent time delays, *Dyn. Games Appl.* **10**, 664 (2020).
  - [12] A. Traulsen, M. A. Nowak, and J. M. Pacheco, Stochastic dynamics of invasion and fixation, *Phys. Rev. E* **74**, 011909 (2006).
  - [13] H. Ohtsuki, M. A. Nowak, and J. M. Pacheco, Breaking the symmetry between interaction and replacement in

- evolutionary dynamics on graphs, *Phys. Rev. Lett.* **98**, 108106 (2007).
- [14] X. Chen, A. Szolnoki, and M. Perc, Risk-driven migration and the collective-risk social dilemma, *Phys. Rev. E* **86**, 036101 (2012).
- [15] J. Hofbauer and K. Sigmund, *Evolutionary Games and Population Dynamics* (Cambridge University Press, Cambridge, 1998).
- [16] K. Sigmund, *The Calculus of Selfishness* (Princeton University Press, Princeton, NJ, 2010).
- [17] J. Alboszta and J. Miekisz, Stability of evolutionarily stable strategies in discrete replicator dynamics with time delay, *J. Theor. Biology* **231**, 175 (2004).
- [18] See Supplemental Material at <http://link.aps.org/supplemental/10.1103/782p-l2bq> for additional figures and details of the Linear Response Theory for the Replicator Equation with multiple incremental delays, based on which Figs. 3(a) and 4 were generated.
- [19] J. Miekisz and M. Bodnar, Evolution of populations with strategy-dependent time delays, *Phys. Rev. E* **103**, 012414 (2021).
- [20] V. V. Vasconcelos, F. C. Santos, J. M. Pacheco, and S. A. Levin, Climate policies under wealth inequality, *Proc. Natl. Acad. Sci. USA* **111**, 2212 (2014).
- [21] V. V. Vasconcelos, F. C. Santos, and J. M. Pacheco, A bottom-up institutional approach to cooperative governance of risky commons, *Nat. Clim. Change* **3**, 797 (2013).
- [22] J. M. Pacheco, Impact of multiple delays on the governance of risky commons, Zenodo (2025), <https://zenodo.org/records/15604222>.

# Impact of multiple delays on the governance of risky commons

Ana M. Nunes <sup>1</sup> Francisco C. Santos <sup>2,3</sup> and Jorge M. Pacheco <sup>3</sup>

<sup>1</sup>BioSystems and Integrative Sciences Institute, and Departamento de Física,

Faculdade de Ciências da Universidade de Lisboa Campo Grande, 1749-016 Lisboa, Portugal

<sup>2</sup>INESC-ID and Instituto Superior Técnico, Universidade de Lisboa, 2744-016 Porto Salvo, Portugal

<sup>3</sup>ATP-Group, P-2744-016 Porto Salvo, Portugal

## SUPPLEMENTAL MATERIAL

### 1. Supplementary Figures

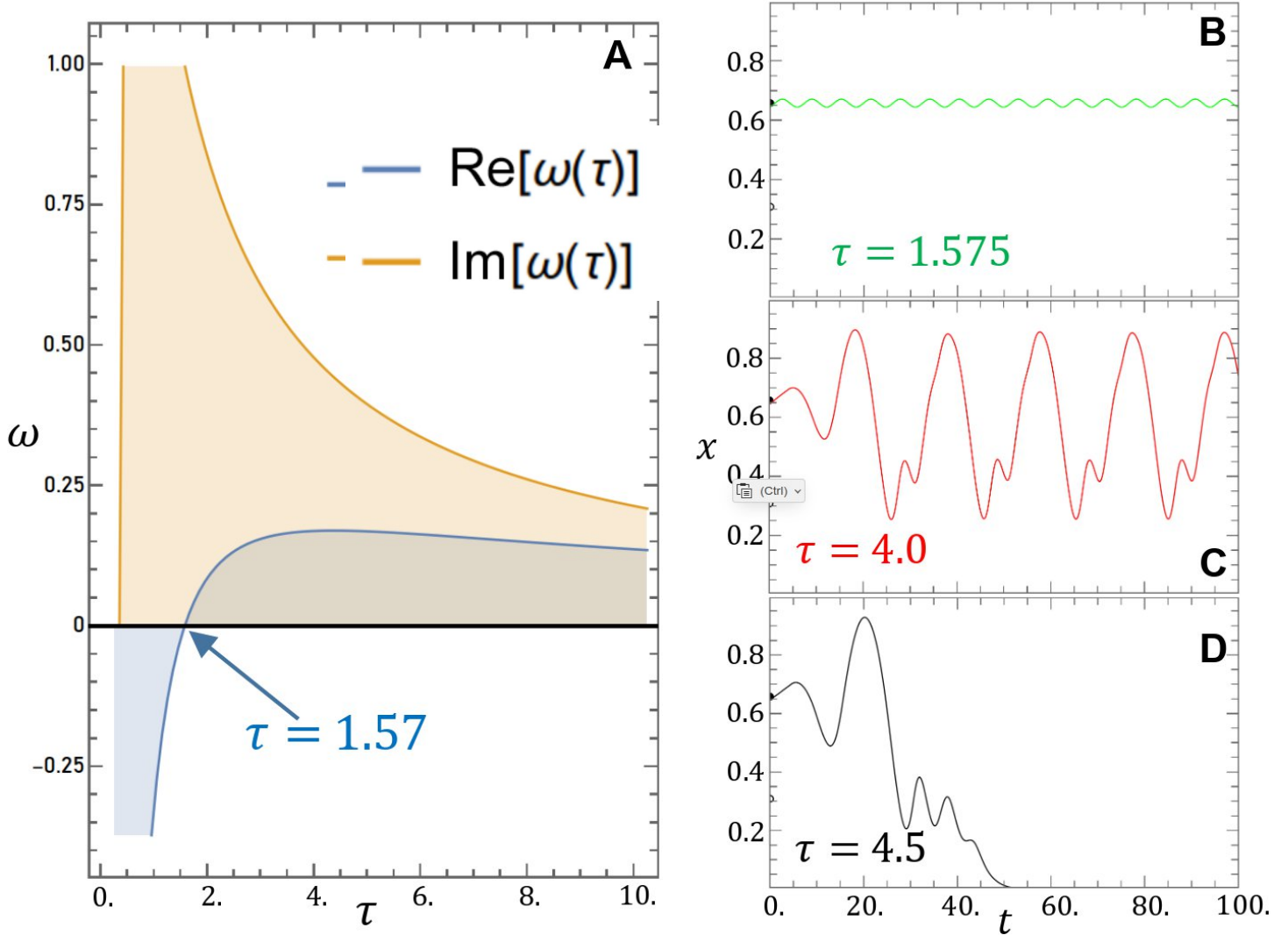


**Figure S1 Linear Response predictions and numerical simulations.** **A.** Linear Response Theory assumes that deviations from the **IS** behave as  $y = e^{\omega t}$  where  $\omega$  becomes a (complex) function of the delay  $\tau$ . The panel illustrates the behaviour of the real and imaginary parts of  $\omega(\tau)$ . When  $\tau = \tau_c = 1.57$  a Hopf bifurcation occurs, as the real part of  $\omega$  crosses zero, leading to stable oscillations around the **IS** whose frequency is expected to decrease with increasing  $\tau$ . **B.** Numerical integration of Eq. (2) for  $\tau = 1.575$ , right above the Hopf bifurcation, exhibiting undamped oscillations in the vicinity of the **IS** (indicated with a black solid semicircle – with the **IU** indicated with a black open semicircle). **C.** and **D.** Same as **B** computed for higher values of  $\tau$  showing that, for  $\tau \geq 7$  the **IS** is no longer stable. In all panels we used the parameters  $b = 5.295$ ,  $c = 0.1$ ,  $N = 8$ ,  $M = 5$ ,  $\sigma = 0.75$ .



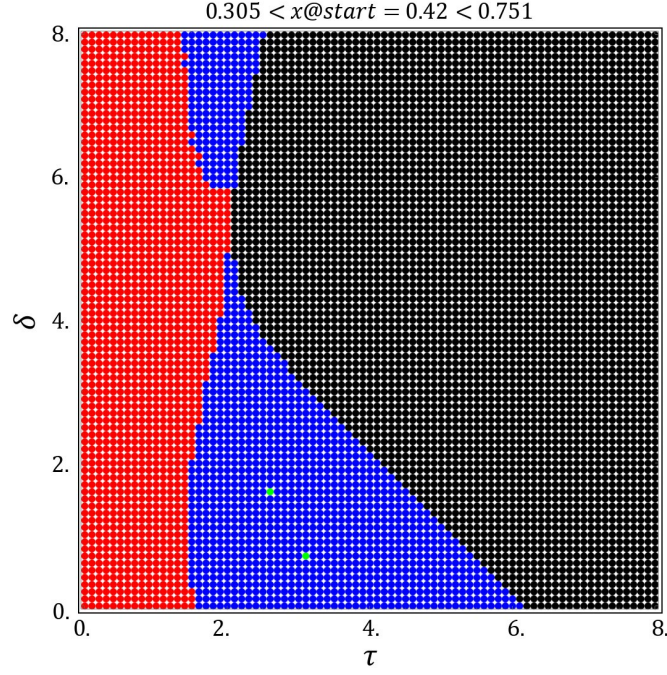


**Figure S2 Long term time integration of Eq. (2).** Time integration of Eq. (2) was carried out for a long time period ( $t = 10000$ ). We used the parameters of Fig. 1 and selected a discrete grid of delay values, where  $0 \leq \{\tau, \delta\} \leq 8$  using  $\Delta\tau = \Delta\delta = 0.1$ . Besides the time integration we also performed a Fast Fourier Transform of the time series after discarding a first transient up to  $t = 1000$ . This way, we can easily identify the long term attractors of the system, be they single points (such as **IS** or **DS**), periodic orbits, or chaotic attractors, whose signature is, asymptotically, associated with aperiodic behaviour. Relaxation (with or without damped oscillations) to the **IS** is represented by red solid circles; Undamped oscillations around the **IS** are represented with solid blue circles; Relaxation (with or without damped oscillations) to the **DS** are shown with black solid circles; Finally, green solid circles indicate instability of the numerical integration algorithm. The results shown here correspond to start from an initial fraction of cooperators indicated at the top of the panel, reproducing the left panel of Fig. 5.

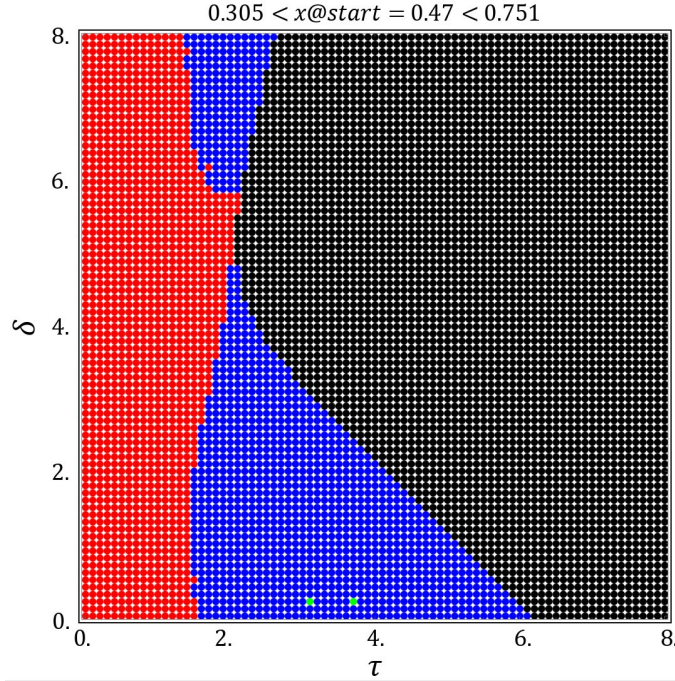


**Figure S3 Long term time integration of Eq. (2).** Time integration of Eq. (2) using the same notation and game parameters of Fig S1. The results shown here correspond to start from an initial fraction of cooperators indicated at the top of the panel.

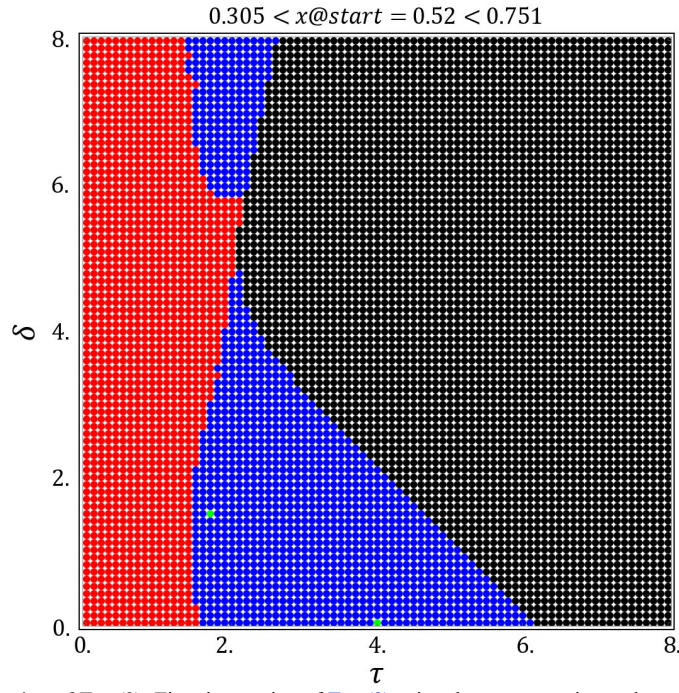


**Figure S4** Long term time integration of Eq. (2). Time integration of Eq. (2) using the same notation and game parameters of Fig S1. The results shown here correspond to start from an initial fraction of cooperators indicated at the top of the panel.

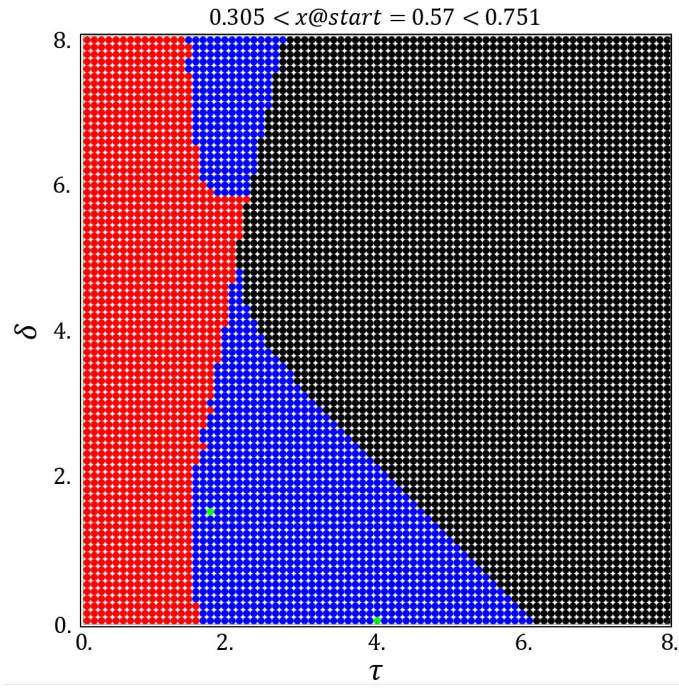


**Figure S5** Long term time integration of Eq. (2). Time integration of Eq. (2) using the same notation and game parameters of Fig S1. The results shown here correspond to start from an initial fraction of cooperators indicated at the top of the panel.



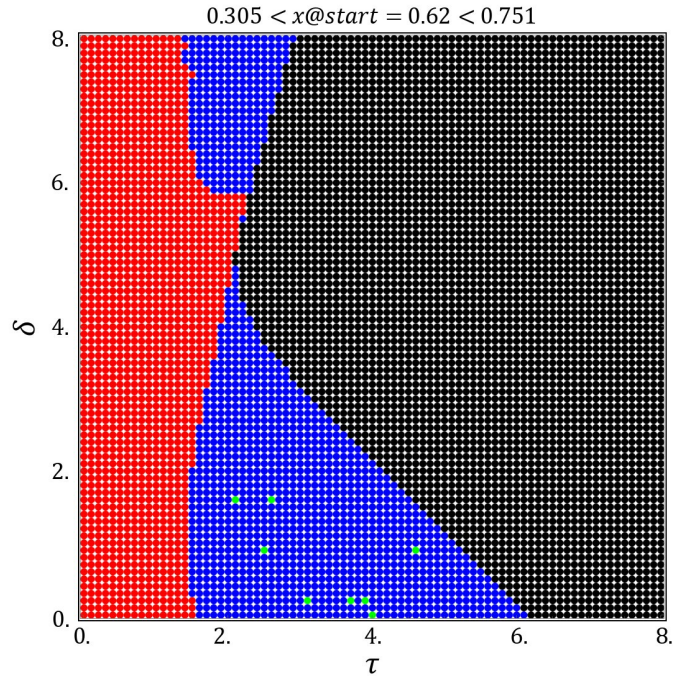


**Figure S6 Long term time integration of Eq. (2).** Time integration of Eq. (2) using the same notation and game parameters of Fig S1. The results shown here correspond to start from an initial fraction of cooperators indicated at the top of the panel.

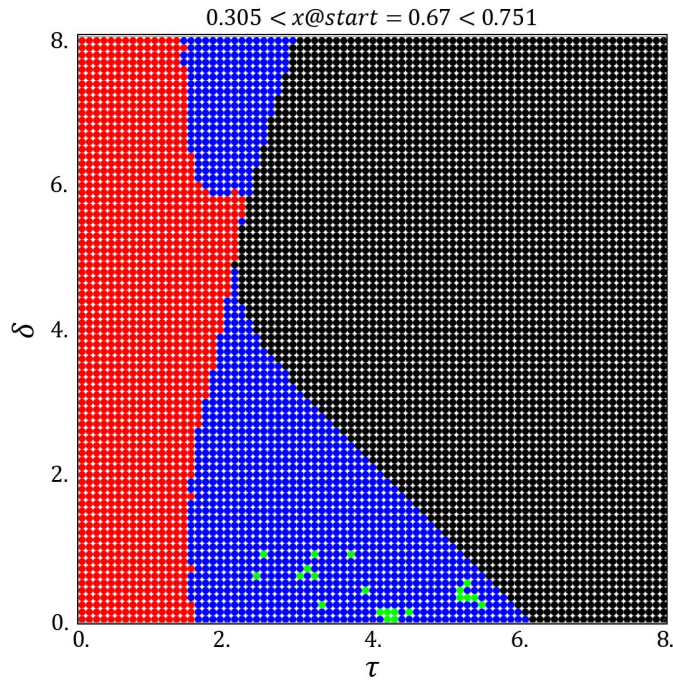


**Figure S7 Long term time integration of Eq. (2).** Time integration of Eq. (2) using the same notation and game parameters of Fig S1. The results shown here correspond to start from an initial fraction of cooperators indicated at the top of the panel.

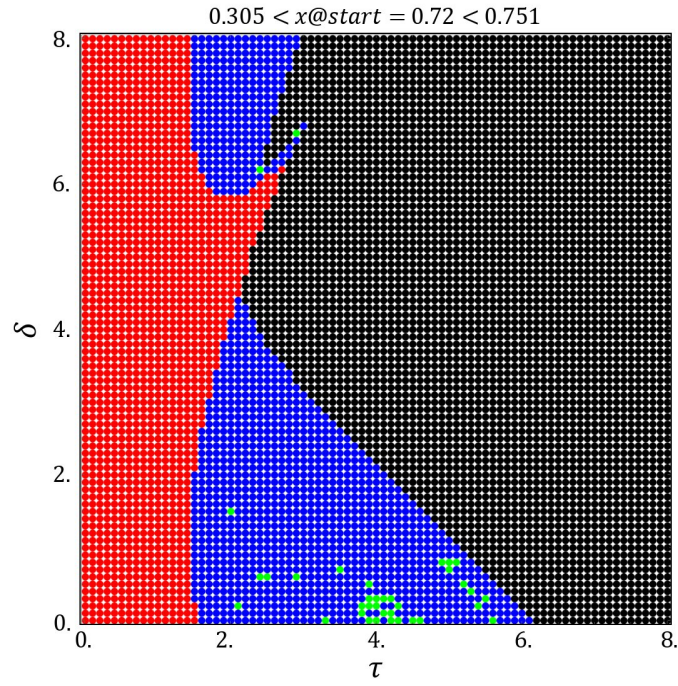


**Figure S8 Long term time integration of Eq. (2).** Time integration of Eq. (2) using the same notation and game parameters of Fig S1. The results shown here correspond to start from an initial fraction of cooperators indicated at the top of the panel.

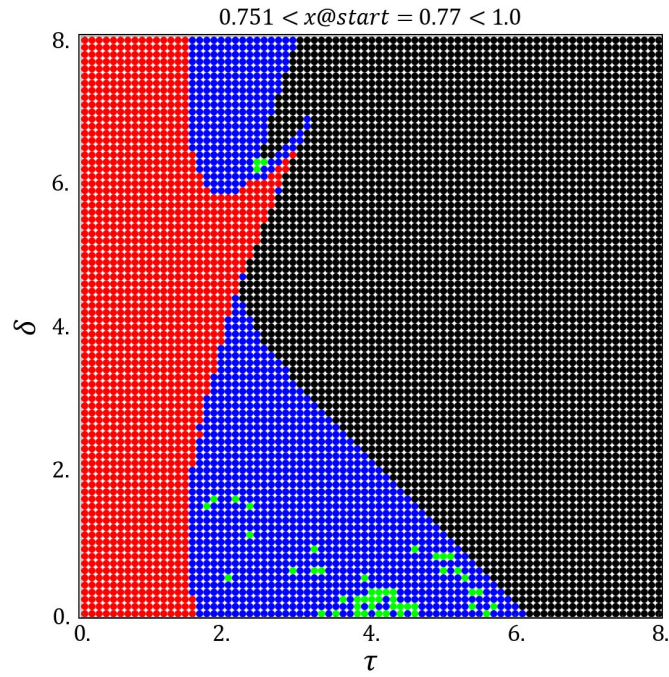


**Figure S9 Long term time integration of Eq. (2).** Time integration of Eq. (2) using the same notation and game parameters of Fig S1. The results shown here correspond to start from an initial fraction of cooperators indicated at the top of the panel, reproducing the middle panel of Fig. 5.



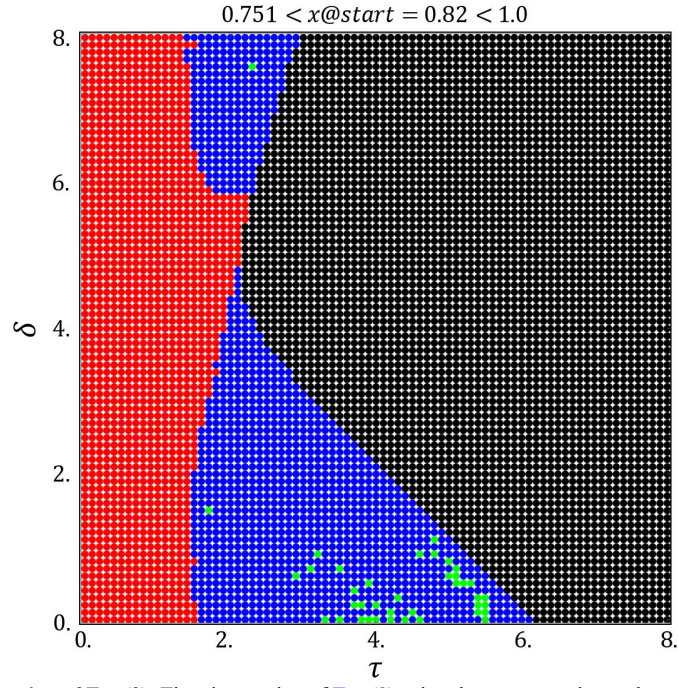


**Figure S10 Long term time integration of Eq. (2).** Time integration of Eq. (2) using the same notation and game parameters of Fig S1. The results shown here correspond to start from an initial fraction of cooperators indicated at the top of the panel.

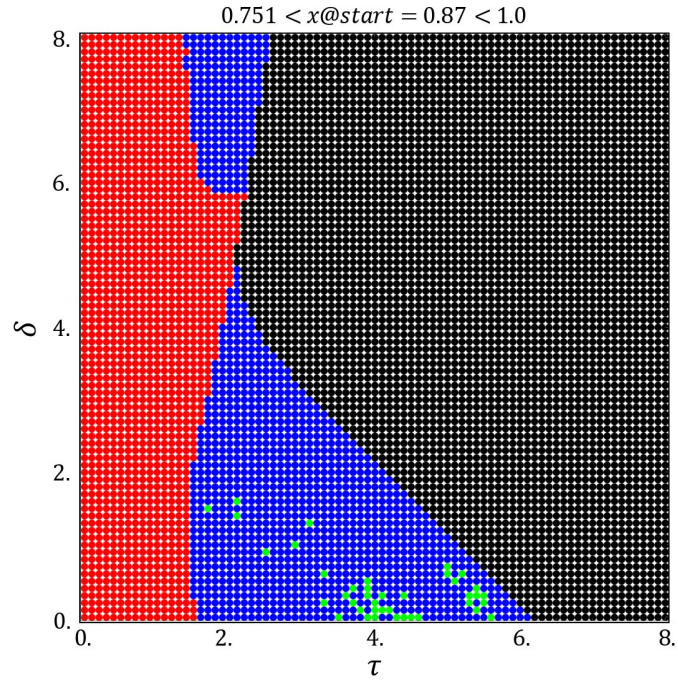


**Figure S11 Long term time integration of Eq. (2).** Time integration of Eq. (2) using the same notation and game parameters of Fig S1. The results shown here correspond to start from an initial fraction of cooperators indicated at the top of the panel.

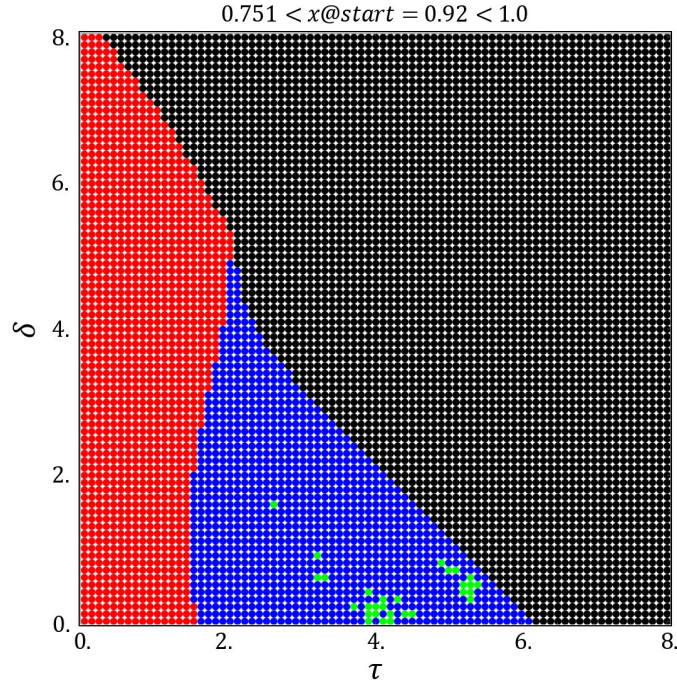


**Figure S12 Long term time integration of Eq. (2).** Time integration of Eq. (2) using the same notation and game parameters of Fig S1. The results shown here correspond to start from an initial fraction of cooperators indicated at the top of the panel, reproducing the right panel of Fig. 5.

## 2. Linear Response Theory for the Replicator Equation with (multiple) delays

### 2.1. Notation & definitions

Linearization around a fixed point  $x^*$  assumes

$$x(t) = x^* + y(t) \Leftrightarrow x_t = x^* + y_t$$

$$x(t - \tau) = x^* + y(t - \tau) \Leftrightarrow x_\tau = x^* + y_\tau$$

$$x(t - v) = x^* + y(t - v) \Leftrightarrow x_v = x^* + y_v$$

with the consideration of these 2 possible delays as discussed in the main text,  $\tau$  and  $v$ , the Replicator Equation (**RE**) reads

$$\dot{x}(t) = x(t)(1 - x(t))(f^C(x(t - \tau), x(t - v)) - f^D(x(t - \tau), x(t - v)))$$

or

$$\dot{x}_t = x_t(1 - x_t)(f^C(x_\tau, x_v) - f^D(x_\tau, x_v))$$

with

$$f^C(x_\tau, x_v) = \sum_{k=0}^{N-1} C_{N,k}(x_\tau) \Pi^C(k + 1, x_v)$$

$$f^D(x_\tau, x_v) = \sum_{k=0}^{N-1} C_{N,k}(x_\tau) \Pi^D(k, x_v)$$

where

$$C_{N,k}(x_\tau) = \binom{N-1}{k} x_\tau^k (1-x_\tau)^{N-1-k}$$

Finally, we shall make the replacement

$$y_t = y(t) = e^{\omega t}$$

and, naturally

$$y_\tau = y(t - \tau) = e^{\omega(t-\tau)}$$

$$y_v = y(t - v) = e^{\omega(t-v)}$$

where  $\omega = x + i y$  is a complex quantity (in general), and will depend on  $\tau$  and  $v$ . Our goal here is to determine  $\omega$ .

## 2.2. The RF-CRD model

Let us take the **RF-CRD** model with adaptive risk and different delays; we have the following payoffs

$$\Pi^D(k, x_v) = b \theta(k - M) + [1 - \theta(k - M)] b (1 - r [\eta(N, M, x_v)])$$

$$\Pi^C(k, x_v) = \Pi^D(k, x_v) - cb$$

where  $\theta(k - M)$  is the usual Heaviside distribution, with  $\theta(k - M) = 0$  if  $k < M$  and 1 otherwise. We have further that

$$\eta(N, M, x_v) = \sum_{k=M}^N \binom{N}{k} x_v^k (1-x_v)^{N-k}$$

and

$$r [\eta(N, M, x_v)] = [1 - \eta(N, M, x_v)]^\sigma$$

The model parameters we shall explore are  $b = 5.475$ ,  $\frac{c}{b} = 0.1$ ,  $N = 8$ ,  $M = 5$ ,  $\sigma = 0.25$ , leading to the evolutionary dynamics portrayed in [Fig. 2](#) of main text. Note that the location of the fixed points of the dynamics depends, for a given value of  $\sigma$ , only on the ratio  $c/b$ . This way, we fix the absolute value of  $b$  in such a way that the relaxation time due to small deviations from the **IS** in the absence of delay satisfies  $\tau_\omega \sim 1/\omega \sim 1$  time unit, thus providing a natural time scale with which to compare critical delay values obtained theoretically. For the parameter values above, we obtain, for the location of the fixed points, the values  $x(\mathbf{IU}) = 0.305$  and  $x(\mathbf{IS}) = 0.751$ . In the following, we shall linearize the **RE** in the vicinity of the **IS**. For generic values of the parameters, away from bifurcation points, the linearized system describes the behavior of the solutions close to the **IS**.

## 2.3. Linearizing the RE with the same delay in all terms ( $v = \tau$ , instantaneous risk assessment )

Employing the definitions in [2.1](#), substitution in the **RE**

$$\dot{x}_t = x_t(1 - x_t)(f^C(x_t) - f^D(x_t))$$

and keeping terms up to first order in  $y_t$  and  $y_\tau$  leads to

$$\dot{y}_t = \chi y_\tau \tag{S1}$$

with

$$\chi = x^*(1 - x^*) \left( f_{x_\tau}^C(x^*, x^*) - f_{x_\tau}^D(x^*, x^*) \right)$$

where we defined

$$f_{x_\tau}^{C|D}(x^*) = \left( \frac{\partial f^{C|D}}{\partial x_\tau} \right)_{(x_t=x^*)}$$

For  $\sigma = 0.25$  and game parameters above we obtain  $\chi = -0.999$ .

### 2.3.1. Looking for a solution to the linearized problem

We try solutions for [Eq. S1](#) of the form

$$y_t = y(t) = e^{\omega t} \text{ and } y_\tau = y(t - \tau) = e^{\omega(t - \tau)}$$

Substituting in [Eq. S1](#) we obtain

$$\omega e^{\omega t} = \chi \tau$$

This equation can be solved analytically making use of the Lambert  $W$ -function, leading to

$$\omega \equiv \alpha + i\beta = \frac{1}{\tau} W(\chi \tau)$$

Since  $\chi < 0$ , 2 regimes emerge from the expression above :

1. whenever  $\chi \tau$  satisfies  $-\frac{1}{e} \leq \chi \tau < 0$  then  $\omega$  is a negative real number and we obtain an exponential decay to  $x^*$ ;
2. whenever  $\chi \tau < -\frac{1}{e}$  then  $\omega$  becomes complex with positive imaginary part, such that i) for  $-\frac{\pi}{2} < \chi \tau < -\frac{1}{e}$  we obtain damped oscillations towards  $x^*$ ; ii) for  $\chi \tau = -\frac{\pi}{2}$  and we obtain sustained (undamped) oscillations around  $x^*$  (zero real part, corresponding to the Hopf bifurcation); iii) for  $\chi \tau < -\frac{\pi}{2}$ , the real part becomes positive and we obtain oscillations of growing amplitude around  $x^*$ .

At the Hopf bifurcation the solution can be written

$$y(t) = e^{i \frac{\pi}{2\tau_c} t}$$

### 2.4. Linearizing the RE with multiple delays (non-instantaneous risk assessment )

Employing again the definitions in [2.1](#), substitution in the **RE**



$$\dot{x}_t = x_t (1 - x_t) (f^C(x_t, x_v) - f^D(x_t, x_v))$$

and keeping terms up to first order in  $y_t$ ,  $y_\tau$  and  $y_v$  leads to

$$\dot{y}_t = \phi y_\tau + \psi y_v \quad (\text{S2})$$

with

$$\phi = x^* (1 - x^*) (f_{x_\tau}^C(x^*, x^*) - f_{x_\tau}^D(x^*, x^*))$$

and

$$\psi = x^* (1 - x^*) (f_{x_v}^C(x^*, x^*) - f_{x_v}^D(x^*, x^*))$$

where we further defined

$$f_{x_v}^{C|D}(x^*) = \left( \frac{\partial f^{C|D}}{\partial x_v} \right)_{(x_v=x^*)}$$

#### 2.4.1. Looking for a solution to the linearized problem

We try solutions for [Eq. S2](#) of the form

$$y_t = y(t) = e^{\omega t}, y_\tau = y(t - \tau) = e^{\omega(t - \tau)} \text{ and } y_v = y(t - v) = e^{\omega(t - v)}$$

Substituting in [Eq. S2](#) we obtain

$$\omega - \phi e^{-\omega \tau} - \psi e^{-\omega v} = 0 \quad (\text{S3})$$

This generalized characteristic equation is hard to solve analytically for the general case, and was solved numerically using the software *Mathematica*. The results are shown in [Fig. 4](#) of main text.